CrystEngComm

Accepted Manuscript

ROYAL SOCIETY OF CHEMISTRY

www.rsc.org/crystengcomm

Journal Name

RSCPublishing

ARTICLE

Calcite nucleation on the surface of PNIPAM-PAAc micelles studied by time resolved *in situ* PXRD

Cite this: DOI: 10.1039/x0xx00000x

Anders C. S. Jensen,[a] Mogens Hinge[b] and Henrik Birkedal[a] ,

Received 00th January 2012,
Accepted 00th January 2012

DOI: 10.1039/x0xx00000x

www.rsc.org/

Biominerals such as $CaCO_3$ have been studied extensively in an effort to replicate materials found in Nature. But understanding and controlling the formation of $CaCO_3$ has proved a challenge for example in regards to control over crystallite size. The formation of pure calcite has been studied to some degree and a myriad of materials are made utilizing organic additives to control morphology, polymorphism and crystallite size. In this work, these aspects were combined by applying PNIPAM-b-PAAc micelles as control agents for calcite crystallization. The crystallization mechanism in this system was studied by time resolved *in situ* PXRD. This revealed that crystalline nanoplatelets of calcite were formed on the surface of the polymer particles . Higher concentration of polymer lead to purely crystalline calcite nanoplatelets with complete inhibition of growth of larger crystallites.

Introduction

Biominerals are formed with specific morphology and polymorphism under strict biological control. These materials make up the structural support of many organisms[1]. One of the most studied biominerals is calcite, which is found in many marine life forms[2]. Calcite formation has been studied studied in both biogenic and a wide range of synthetic samples[3-10]. Many advancements have recently been made in the understanding of calcium carbonate nucleation pathways in general; these studies have highlighted prenucleation behaviour and amorphous precursor phases[10-19].

From the studies of synthetic calcite the effects of various organic additives have been elucidated. For example, Borukhin *et al*. revealed, while studying the incorporation of amino acids, that carboxylate and thiol groups interact strongly with $CaCO_3$[20]. To emulate the proteins often found in biogenic samples, synthetic polymeric additives have been applied[21]. In general polymers, especially block copolymers, provide excellent opportunities for controlling crystallization[10, 22, 23]. These studies showed that poly(acrylic acid) (PAAc) stabilizes amorphous calcium carbonate (ACC)[24, 25]. Various copolymers like ABA block-copolymers have been applied forming both simple spherical particles[26] and more complex superstructures[27]. Spherical $CaCO_3$ have been made with a range of advanced polymers such as dendrite polymer[28] and responsive polymers[29, 30]. Studies using PEG-b-poly(Asp) and PEG-b-poly(Glu) as additives found long Asp and Glu chains produced vaterite while short chains produced calcite[30]. The many studies showing extensive morphological control over $CaCO_3$ prompt the questions of how additives affect the nucleation and growth kinetics of the mineral phase especially with these advanced synthetic polymeric additives that present surfaces in suspension. The crystallization kinetics of $CaCO_3$ has been studied extensively without additives. The most powerful techniques for this purpose include time resolved *in situ* powder x-ray diffraction (PXRD)[31, 32] and transmission electron microscopy (TEM)[18, 19]. These studies show that calcite generally forms in one of two ways: either directly from an amorphous precursor:

$$\mathrm{ACC}(s) \rightarrow \mathrm{calcite}(s)$$

or via a vaterite precursor:

$$\mathrm{ACC}(s) \rightarrow \mathrm{vaterite}(s) \rightarrow \mathrm{calcite}(s)$$

Blanco *et al*. showed that the vaterite phase takes several hours to transform into calcite if present and the kinetics of crystallization depend crucially on e.g. temperature[32].

Herein we formed an organic surface in suspension and used it to direct the growth of calcite to achieve formation of nanocrystalline calcite (NCC). The formation kinetics were studied by time resolved *in situ* PXRD. To form the organic surface, we employed the thermo-responsive block copolymer poly(*N*-isoprolyacrylamide-b-acrylic acid) (PNIPAM-b-PAAc).

The PNIPAM block has a lower critical solution temperature at which it's effective solubility changes drastically resulting in a conformational change of the polymers and has been extensively investigated for use in biomedical applications[33-35]. The PAAc was used to interact with calcium ions. The PNIPAM block thus only acts as scaffolding while the PAAc block emulates the action of acidic macromolecules of biomineralization. The PNIPAM-b-PAAc was characterized by DLS and turbidity, to determine the behaviour of the micelles in the presence of calcium ions that has previously been reported to change the behaviour of similar polymers[36]. The kinetics of crystallization was investigated using *in situ* synchrotron powder diffraction[31, 32, 37-39] showing that increasing polymer concentration lead to purely nanocrystalline calcite.

Experimental

Polymer synthesis. The synthesis of PNIPAM-b-PAAc was based on a one pot surfactant free emulsion polymerization synthesis developed by Hinge[40]. In brief, 500 mL of purified water was flushed with N_2 to remove O_2. 0.3 g potassium persulfate (≥99% Sigma-Aldrich) and 6.25 g of NIPAM (97% Sigma Aldrich) was dissolved in the water. The solution was heated to 70 °C and after 30 min or after the solution turned opaque 1 mL AAc (99% Sigma Aldrich) was added to achieve a 15 wt% PAAc. The 4-hydroxy anisole inhibitor was removed from the AAc by passing the monomer trough an Al_2O_3 column prior to addition. After 24 hr of polymerization and the polymers was purified by dialysisusing a spectra/Por® dialysis Membrane MWCO: 3.500 (spectrum laboratories, inc.) against deionised (DI) water for 7 days with water changed daily. FTIR measurement showed that the no unreacted monomers were left in the sample after purification (Figure S1, see supplementary material).

Particle synthesis. All sample were made by mixing 10 ml of 0.06 M $CaCl_2{\cdot}2H_2O$ (>99% Sigma Aldrich) with 10 ml of PNIPAM-b-PAAc solutions with polymer concentrations of 0-0.4 mg/mL. 10 ml of 0.06 M $NaHCO_3$ (>99% Sigma Aldrich) and 0.06 M NaOH (>98% Sigma Aldrich) was added. The reaction was kept at the desired temperature for 24 h, using a Julabo ED/F 12 and a water bath with a MIXdrive 15 2Mag magnetic stirrer. All samples were purified by dialysis using the same membrane as for polymer purification for 24 h against DI water and centrifuged. The samples were dried at 60 °C overnight.

Characterization. All $CaCO_3$ samples where characterized by PXRD and scanning electron microscopy (SEM). For PXRD, a Rigaku Smartlab diffractometer (Rigaku corporation, Tokyo, Japan) with a Cu *Kα* rotating anode was used in parallel beam focusing mode. The samples were mounted on a flat sample spinner and spun at 30 rpm. A LaB_6 standard (NIST) was used to account for the instrumental line broadening. Rietveld refinement was done in Fullprof[41] using spherical harmonics to model crystallite size anisotropy[42]. SEM micrographs were recorded on a Nova nanoSEM 600 (FEI, Eindhoven, The Netherlands) with an ETD detector. FTIR analysis was carried out on a Nicolet 380 FTIR (Thermo ficher Scientific) with an ATR module and a wavenumber range of 400-4000 cm^{-1} and a resolution of 4 cm^{-1}.

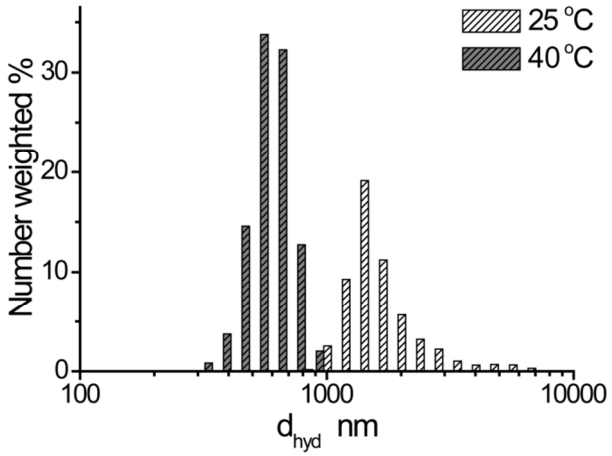

Figure 1. DLS measurement of PNIPAM-b-PAAc below (25 °C, light gray) and above the LCST (40 °C, dark gray), respectively.

The turbidity experiments were conducted on a Perkin Elmer (Waltham, MA, US) Lambda 25 UV/VIS spectrometer. The temperature was ramped at 1 °C/min, controlled by a Perkin Elmer PTP-Peltier system (Waltham, MA, US) with a circulating water thermostat (Julabo F12/ED hydrostatic bath, Seelbach, Germany) to remove excess heat from the peltier device. The samples were measured at 600 nm with 0.1 °C temperature resolution in the desired temperature range that was adapted to encompass the LCST transition behavior for each system. The samples were prepared by dissolving ~0.1 mg polymer in 3 mL of demineralized water and measured in a quartz cuvette. DLS experiments were performed on a Nanoflex 180° using the Microtrac flex 11.0.0.2 software (Microtrac, PA, USA). Samples were measured 10 times with a run time of 120 s using a Julabo F12/ED hydrostatic bath for temperature control (Julabo, Seelbach, Germany).

***In situ* PXRD characterization.** The *in situ* PXRD study was performed at MAXlab (Lund, Sweden) at the i711 beam line[43]. A LaB_6 standard was used for calibration. The wavelength was refined to 0.9909 Å and the sample to detector distance was set to 80 mm. A 2D Titan CCD detector (Agilent Technologies, Santa Clara, USA) was used for data acquisition. A diffractogram was recorded every 22 s with an exposure time of 17 s. The sample was held in a single crystal sapphire capillary with an inner diameter of 0.9 mm, according to the setup developed by Ibsen *et al.*[37]. Equal amounts of the calcium (0.8 M $CaCl_2$ (>99% Sigma Aldrich)) and carbonate solutions (0.8 M $NaHCO_3$ (>99% Sigma Aldrich) and 0.8 M NaOH (>98% Sigma Aldrich), i.e. 0.8 M Na_2CO_3.) were pumped into the capillary by a peristaltic pump. The calcium solution was mixed with varying amounts of PNIPAM-b-PAAc.

The 2D diffractogram were integrated with Fit2D[44] and refined in GSAS[45, 46]. The diffraction patterns were dominated by a large background due to diffuse scattering from water and amorphous phases. It was fitted by a 28-degree Chebyshev polynomial, similar to the approach used by Ibsen *et al*.[37]. The calcite phase was fitted by a calcite model[47].

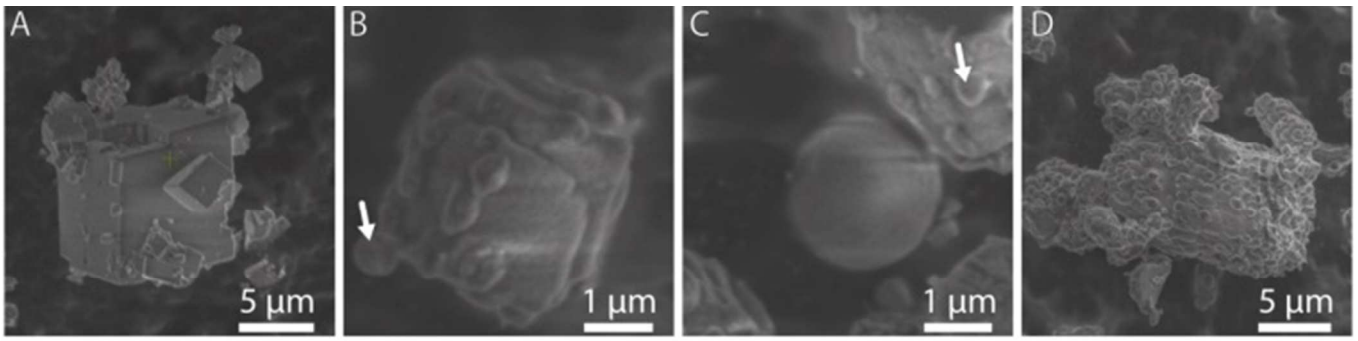

Figure 2. Representative SEM micrographs of $CaCO_3$ prepared without the polymer (A), at intermediate (0.1-0.2 mg/mL) polymer concentration (B-C) and at high (0.4 mg/mL) polymer concentration (D).

Results & discussion

PNIPAM-b-PAAc polymers. The LCST was determined by turbidity measurements to be 32 and 31 °C for PNIPAM and PNIPAM-b-PAAc, respectively (Figure S2, see supplementary material) showing that the PAAc block had negligible effects on the LCST. Turbidity measurements were also carried out in the presence of $CaCl_2$ and Na_2CO_3 to insure that the responsive behaviour of the PNIPAM block was unaffected by the ions. The sharp transition was maintained in the presence of low concentrations of $CaCl_2$, but broadened significantly to extend over several degrees in the presence of Na_2CO_3. At higher concentration of $CaCl_2$ the LCST was lowered at concentration higher than 0.1 M. However, the LCST remained above 25 °C even at concentrations as high as 0.4 M (Figure S3, see supplementary material). Therefore, the polymer was mixed with the $CaCl_2$, rather than Na_2CO_3 prior to precipitating $CaCO_3$.

DLS experiments showed that the polymer formed mesoscale assemblies above (35 °C) and below (25 °C) the LCST (Figure 1), presumably micelles. The decrease in size upon increasing temperature is due to the PNIPAM block expelling the solvent as it undergoes the LCST transition. DLS experiments was also conducted in the presence of $CaCl_2$ at concentration of 2-400 mM, as ions are known to have influence PNIPAM's LCST[36]. Below the LCST there was no change in the micelle size, but above the LCST the apparent micelle size drops in some experiments due to aggregation; this aggregation is expected from charge neutralization according to DLVO theory (Figure S4, see supplementary material). However, this aggregation behaviour was found to be slow compared to the precipitation of $CaCO_3$. Hence it was possible to circumvent severe aggregation above the LCST by adding Na_2CO_3 immediately after the LCST transition occurs.

$CaCO_3$/PNIPAM-b-PAAc particles. Hybrid $CaCO_3$/PNIPAM-b-PAAc particles were analysed by SEM and PXRD. SEM micrographs showed that without the polymer present rhombohedral $CaCO_3$ particles as expected from calcite crystals were formed (Figure 2 A). At intermediate polymer concentrations (0.1-0.2 mg/mL) a mix of three distinct morphologies was observed, rhombohedral crystals (Figure 2B), ~100 nm spherical particles (Figure 2B-C arrows) and ~1 µm particles (Figure 2C). The rhombohedral crystals are most likely calcite crystals, possibly with some polymer incorporated. The small spherical particles are unlikely to be mineralized polymer micelles as they are smaller than the polymer micelles themselves as observed by DLS (Figure 1). However, the larger spherical particles are consistent with mineralized polymer micelles. At high polymer concentration (0.4 mg/mL) the larger spherical particles are formed exclusively (Figure 2D). These particles are generally found in aggregates a few tens of µm in size. PXRD data (Figure S5, see supplementary material) were fitting by a three phase model.

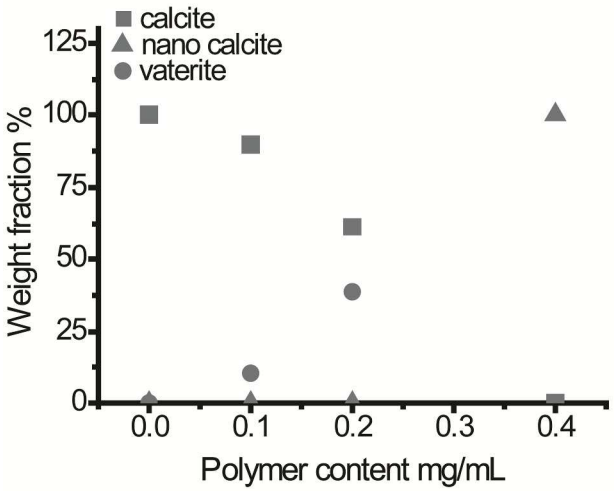

Figure 3. Refined weight fraction of vaterite and calcite determined by Rietveld refinement of *ex situ* PXRD data..

The model described a calcite phase with no line broadening (i.e. macroscopic crystals), a nanocrystalline vaterite phase and NCC. Size induced line broadening could be described for the latter two phases (i.e. crystals below ~100 nm). The refined weight fractions of the three phases are shown in Figure 3. The mix of particles found at intermediate concentration was a mixture of regular macrocrystaline calcite and nanocrystalline vaterite. The NCC phase was only found in the sample at high polymer concentrations. The crystallite size of the NCC was determined from the line broadening to be platelets of 74(3)×43(2) nm in the *a* and *c* direction respectively.

Time resolved *in situ* PXRD was used to study the formation of NCC on the polymeric micelles. These experiments covered a polymer concentration range of 0.34-1.7 g/mL at 0.4 M calcium and carbonate ion concentration, i.e. covering and extending the high concentration regime studied *ex situ* to study the formation mechanisms of NCC. The raw 2D diffractogram showed that both with and without the polymer, calcite was formed (Figure 4 A). By examining the strongest reflection (104) it became clear that the formation of calcite went through a nanocrystalline calcite phase as shown in figure 4B.

$$\mathrm{ACC(s)} \rightarrow \mathrm{NCC(s)} \rightarrow \mathrm{calcite(s)}.$$

Indeed, the first crystalline phase detected is NCC. Only later, peaks from highly crystalline calcite were seen (HCC in Figure 4B).

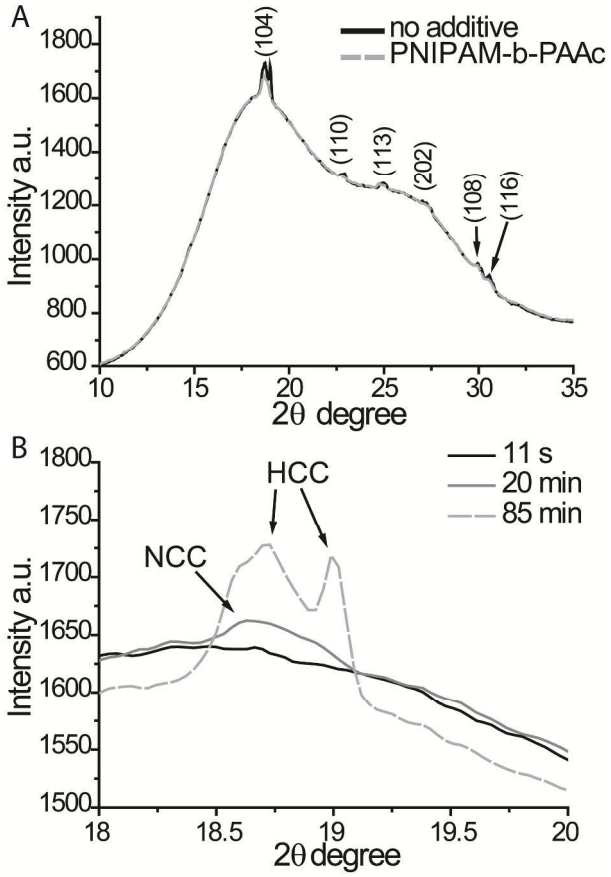

Figure 4. Diffractogram from *in situ* synchrotron diffraction studies of calcite formed with and without polymers present. (A) shows full diffractograms with the observable peaks indexed; the large background originates from water diffraction. (B) Compares the (104) peak region at the beginning, middle and end of the experiment showing how NCC forms first and highly crystalline calcite (HCC) only at late stages.

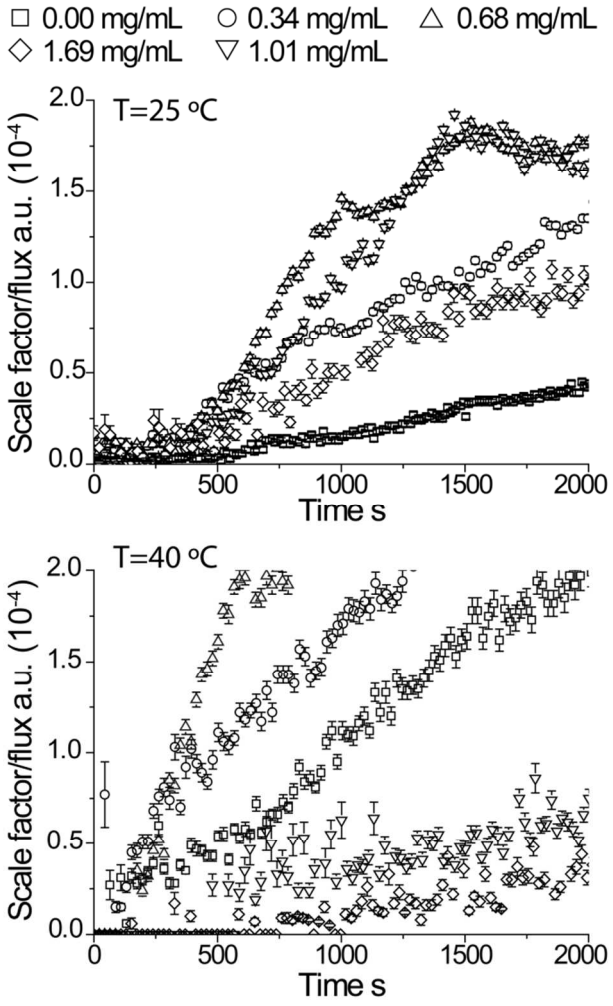

Figure 5. Refined calcite scale factors from the *in situ* synchrotron diffraction study of calcite formation above and below the LCST at various PNIPAM-b-PAAc concentrations. The nucleation of HCC was associated by a sudden change in the slope of the scale factor as indicated by the star for the 0.68 mg/mL sample at 25 °C, the nucleation time of HCC was confirmed by examining the 2D diffraction pattern for single crystal reflections.

As this study focusses on the nucleation of NCC, we only analyse the refined scale factor at times prior to the formation of regular calcite, HCC. The fact that the HCC display peaks at

different diffraction angles than NCC suggest that this phase forms through heterogeneous nucleation on the reactor walls. At the highest polymer concentrations, the regular calcite phase was completely inhibited (1.69 mg/mL at 25 °C and 1.01, 1.69 mg/mL at 40 °C) as seen by the 2D diffractogram in Figure S6 (see supplementary material) meaning that the polymer limits Ostwald ripening by stabilizing the NCC particles[48] and solid-solid interactions[49] that would normally lead to the formation of regular calcite. The scale factor and background were refined for all times (Figure 5).

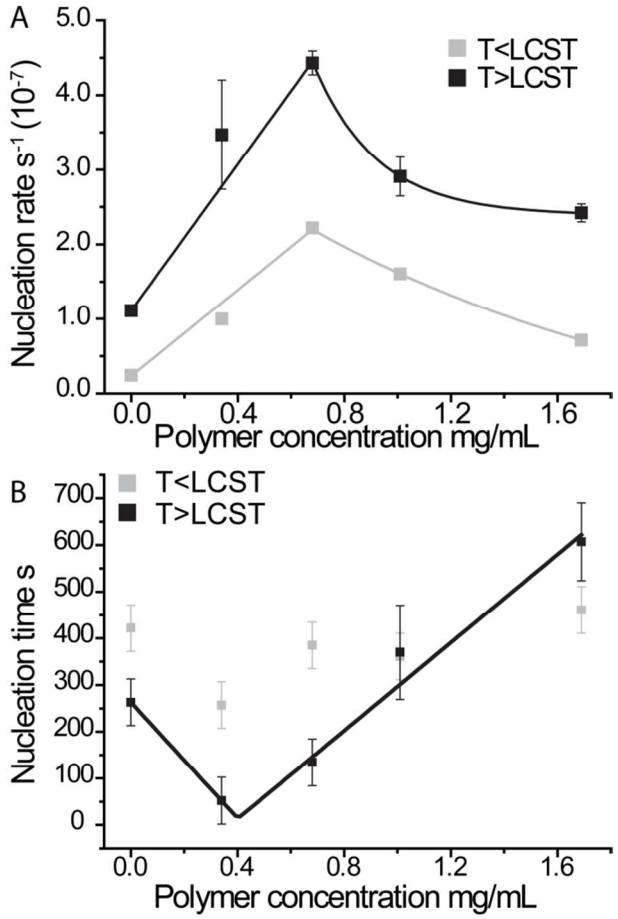

Figure 6. Nucleation rate (A) and nucleation time (B) as a function of polymer concentration determined from the scale factor from Rietveld refinement of *in situ* synchrotron diffraction data. Black and grey symbols are from experiments above and below the polymer LCST, respectively

The unit cell and line broadening were refined at short (seconds after nucleation) and long reaction times (hours after nucleation) and showed no significant change, indicating that the average unit cell and average particles size of the NCC phase does not change as a function of time. The scale factors normalized by incident flux and hence on the same scale are shown in Figure 5. Since the regular calcite form after the NCC phase, the refined scale factor will only be analysed further for times prior to the first HCC peaks becoming visible in the raw data.

The fact that the particle size did not change between beginning and end of the experiment, indicates that the increase in scale factors seen in Figure 5 are caused by nucleation of more NCC crystallites. Hence, the time (t_{nuc}) and rate of nucleation (k_{nuc}) could be determined by fitting the following expression to the refined scale factor:

For $t<t_{\mathrm{nuc}}$

$$scale(t) = c,$$

for $t>t_{\mathrm{nuc}}$

$$scale(t) = k_{\mathrm{nuc}}(t - t_{\mathrm{nuc}}) + c.$$

c is a constant describing the value given by Rietveld refinement when no peaks are present. The thus obtained nucleation rate and nucleation time are highly affected by the polymer additive (Figure 6). The nucleation rate is in all cases higher above LCST than below it. For all investigated polymer concentrations, the nucleation rate is higher than without polymer indicating that PNIPAM-b-PAAc is a nucleation promoter of calcite in this concentration range. At low polymer concentration the nucleation rate greatly increases up to a concentration of 0.7 mg/mL (Figure 6A). This increase is more pronounced in the experiments performed above the LCST. This region was fitted by a straight line, the slope was determined to be $2.9(4)\cdot10^{-7}$ and $4.9(2)\cdot10^{-7}$ $s^{-1}\cdot(mg/mL)^{-1}$. As the particle size does not change as a function of time this is proportional to nucleation events per second per additive concentration. This shows that the calcite nanoplatelets nucleate more rapidly above the LCST suggesting a more facile nucleation on the dehydrated PNIPAM core of the polymer micelle compared to the hydrated PNIPAM core below the LCST. This might be due to the lower effective radius of the PNIPAM core resulting in a higher AAc surface concentration and hence a higher negative charge density on the polymer particle surface. Indeed, the polymer particles reduce in size by about (950 nm/500 nm number average) a factor two. This would correspond to a change in the PAA surface layer of the order of a factor of approximately 3.5 (for calculation see supplementary material), with an ensuing increase in charge density.

At high polymer concentration other effects become dominant and the nucleation rate decreases, but remains higher than without the polymer. Since PAAc is known to stabilize ACC[24], we suggest that ACC stabilization is a main contributor to the reduced nucleation rate at higher concentrations. A higher polymer concentration may also lead to a lower *effective* concentration of free calcium, *i.e.* calcium activity due to calcium chelation. The maximum nucleation rate is, at both temperatures, at 0.68 mg/mL polymer. At 15 wt% AAc, this concentration corresponds to only about 0.0035 carboxylates per calcium ion suggesting that chelation is not likely to be the determining factor. Hence we propose that the maximum in nucleation rate results from a combination of an increasing tendency, resulting from formation of an increased number of

heterogeneous nucleation sites on the polymer particles, and a decreasing tendency originating from the ACC stabilizing capacity of PAAc.

The nucleation time also depends on polymer concentration above the LCST while it display minor variations, essentially within the standard uncertainty, below the LCST (Figure 6B). The nucleation time decreases with added polymer but the increases above a polymer concentration of ~0.4 mg/mL and reaches values above that of the polymer-free system within the concentration range examined. This is consistent with a combination of surface nucleation on the PNIPAM dominating at low polymer concentration and ACC stabilization from PAAc dominating at high concentration. However, one would expect a similar trend below the LCST which is not discernible at the present level of precision. This suggests that there may be other interactions at play that could not be fully resolved in the present experiments.

Conclusions

In this study we have shown that the morphology of calcite crystals can be controlled by responsive co-block polymers such as PNIPMA-b-PAAc. At high polymer concentration we have shown that particle coarsening effects can be completely inhibited within the time frame of our experiments leading to stabilization of nanocalcite. By studying the reaction kinetics by time resolved *in situ* PXRD we found that an organic surfaces such as the PNIPAM-PAAc micelle can have a large effect on the nucleation rate of calcite crystals. Moreover the compactness of the organic scaffold, manipulated by temperature in the present study, can change the efficacy of the surface to affect nucleation events. This was combined with the ACC stabilizing effect of PAAc to control the formation kinetics of the calcite.

Acknowledgements

We thank DANSCATT for funding. We thank the staff of the ID711 beamline for support. We acknowledge Maxlab for provision of synchrotron radiation facilities and we would like to thank Dr. Diana Thomas, Dr. Francisco Javier Casado & Dr. Olivier Balmes for assistance in using beamline ID711. We thank Dr. Casper Ibsen and Ms Vicki Nue for assisting with the *in situ* PXRD experiments and Mr. Thomas Feldberg for assisting with the synthesis of PNIPAM-b-PAAc.

Notes and references

[a] Department of Chemistry & iNANO, Aarhus University, DK-8000 Aarhus C, Denmark.

[b] Department of Engineering, Aarhus University, DK-8000 Aarhus C, Denmark.

† Electronic Supplementary Information (ESI) available: [details of any supplementary information available should be included here]. See DOI: 10.1039/b000000x/

1. S. Mann, *biomineralization*, 1 edn., Oxford University press, Oxford, 2001.
2. E. Bäuerlein, *Angewandte Chemie International Edition*, 2003, **42**, 614-641.
3. Y. Politi, R. A. Metzler, M. Abrecht, B. Gilbert, F. H. Wilt, I. Sagi, L. Addadi, S. Weiner and P. U. P. A. Gilbert, *Proceedings of the National Academy of Sciences*, 2008, **105**, 17362-17366.
4. A. Gal, W. Habraken, D. Gur, P. Fratzl, S. Weiner and L. Addadi, *Angewandte Chemie International Edition*, 2013, **52**, 4867-4870.
5. B. Pokroy, A. N. Fitch, F. Marin, M. Kapon, N. Adir and E. Zolotoyabko, *Journal of Structural Biology*, 2006, **155**, 96-103.
6. H. Leemreize, J. R. Eltzholtz and H. Birkedal, *Eur. J. Miner.*, 2014, **26**, 517-522.
7. H. Leemreize, J. D. Almer, S. R. Stock and H. Birkedal, *J. Roy. Soc. Interf.*, 2013, **10**, 20130319.
8. J. L. Arias and M. S. Fernández, *Chem. Rev.*, 2008, **108**, 4475-4482.
9. M. Cusack and A. Freer, *Chem. Rev.*, 2008, **108**, 4433-4454.
10. N. A. J. M. Sommerdijk and G. de With, *Chem. Rev.*, 2008, **108**, 4499-4550.
11. R. Demichelis, P. Raiteri, J. D. Gale, D. Quigley and D. Gebauer, *Nature Commun.*, 2011, **2**, 590.
12. D. Gebauer, H. Cölfen, A. Verch and M. Antonietti, *Adv. Mater.*, 2009, **21**, 435-439.
13. D. Gebauer, P. N. Gunawidjaja, J. Y. P. Ko, Z. Baczik, B. Aziz, L. J. Liu, Y. F. Hu, L. Bergstrom, C. W. Tai, T. K. Sham, M. Eden and N. Hedin, *Angew. Chem. Int. Ed.*, 2010, **49**, 8889-8891.
14. D. Gebauer, A. Völkel and H. Cölfen, *Science*, 2008, **322**, 1819-1822.
15. J. H. E. Cartwright, A. G. Checa, J. D. Gale, D. Gebauer and C. I. Sainz-Díaz, *Angew. Chem. Int. Ed.*, 2012, **51**, 11960-11970.
16. Y. Politi, Y. Levi-Kalisman, S. Raz, F. Wilt, L. Addadi, S. Weiner and I. Sagi, *Adv. Func. Mater.*, 2006, **16**, 1289-1298.
17. Y. Politi, R. A. Metzler, M. Albrecht, B. Gilbert, F. H. Wilt, I. Sagi, L. Addadi, S. Weiner and P. U. P. A. Gilbert, *Proc. Natl. Acad. Sci. USA*, 2008, **105**, 17362-17366.
18. P. J. M. Smeets, K. R. Cho, R. G. E. Kempen, N. A. J. M. Sommerdijk and J. J. De Yoreo, *Nat. Mater.*, 2015, **14**, 394-399.
19. M. H. Nielsen, S. Aloni and J. J. De Yoreo, *Science*, 2014, **345**, 1158-1162.
20. S. Borukhin, L. Bloch, T. Radlauer, A. H. Hill, A. N. Fitch and B. Pokroy, *Advanced Functional Materials*, 2012, **22**, 4216-4224.
21. Y. Boyjoo, V. K. Pareek and J. Liu, *Journal of Materials Chemistry A*, 2014, **2**, 14270-14288.
22. S.-H. Hu and H. Cölfen, *J. Mater. Chem.*, 2004, **14**, 2124-2147.
23. H. Cölfen, *Methods in Enzymology*, 2013, **532**.
24. Y. Oaki, S. Kajiyama, T. Nishimura, H. Imai and T. Kato, *Advanced Materials*, 2008, **20**, 3633-3637.

25. S.-C. Huang, K. Naka and Y. Chujo, *Langmuir*, 2007, **23**, 12086-12095.
26. K. Tauer, V. Khrenov, N. Shirshova and N. Nassif, *Macromolecular Symposia*, 2005, **226**, 187-202.
27. N. Nassif, N. Gehrke, N. Pinna, N. Shirshova, K. Tauer, M. Antonietti and H. Cölfen, *Angewandte Chemie International Edition*, 2005, **44**, 6004-6009.
28. L. Wang, Z. Meng, Y. Yu, Q. Meng and D. Chen, *Polymer*, 2008, **49**, 1199-1210.
29. X.-H. Guo, S.-H. Yu and G.-B. Cai, *Angewandte Chemie International Edition*, 2006, **45**, 3977-3981.
30. P. Kašparová, M. Antonietti and H. Cölfen, *Colloids and Surfaces A: Physicochemical and Engineering Aspects*, 2004, **250**, 153-162.
31. P. Bots, L. G. Benning, J.-D. Rodriguez-Blanco, T. Roncal-Herrero and S. Shaw, *Crystal Growth & Design*, 2012, **12**, 3806-3814.
32. J. D. Rodriguez-Blanco, S. Shaw and L. G. Benning, *Nanoscale*, 2011, **3**, 265-271.
33. S. Chaterji, I. K. Kwon and K. Park, *Prog. Polym. Sci.*, 2007, **32**, 1083-1122.
34. Y. Guan and Y. Zhang, *Soft Matter*, 2011, **7**, 6375–6384.
35. D. Roy, W. L. A. Brooks and B. S. Sumerlin, *Chem. Soc. Rev.*, 2013, **42**, 7214--7243.
36. X. Liu, S. Luo, J. Ye and C. Wu, *Macromolecules*, 2012, **45**, 4830-4838.
37. C. J. S. Ibsen and H. Birkedal, *Journal of Applied Crystallography*, 2012, **45**, 976-981.
38. G. V. Jensen, M. Bremholm, N. Lock, G. R. Deen, T. R. Jensen, B. B. Iversen, M. Niederberger, J. S. Pedersen and H. Birkedal, *Chemistry of Materials*, 2010, **22**, 6044-6055.
39. C. J. S. Ibsen and H. Birkedal, *Nanoscale*, 2010, **2**, 2478-2486.
40. M. Hinge, *Colloid J*, 2007, **69**, 342-347.
41. J. Rodriguez-Carvajal, *An introduction to the program fullprof 2000*, 2001.
42. M. Jarvinen, *Journal of Applied Crystallography*, 1993, **26**, 525-531.
43. Y. Cerenius, K. Stahl, L. A. Svensson, T. Ursby, A. Oskarsson, J. Albertsson and A. Liljas, *Journal of Synchrotron Radiation*, 2000, **7**, 203-208.
44. A. Hammersley, *European Synchrotron Radiation Facility Internal Report ESRF97HA02T*, 1997.
45. A. Larsen and R. Von Dreele, *LANSCE, MS-H805, Los Alamos National Laboratory, Los Alamos, NM*, 1994.
46. B. H. Toby, *Journal of Applied Crystallography*, 2001, **34**, 210-213.
47. T. Pilati, F. Demartin and C. Gramaccioli, *Acta Crystallographica Section B: Structural Science*, 1998, **54**, 515-523.
48. F. Haußer and E. Lakshtanov, *Physical Review E*, 2012, **86**, 062601.
49. L. N. Schultz, K. Dideriksen, L. Lakshtanov, S. S. Hakim, D. Müter, F. Haußer, K. Bechgaard and S. L. S. Stipp, *Crystal Growth & Design*, 2014, **14**, 552-558.

Table of Contents graphic

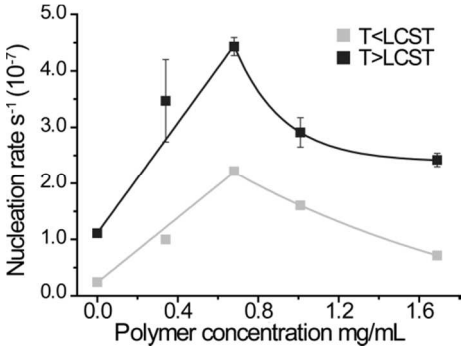

Nanocrystalline calcite is formed under the influence of block copolymers containing thermoresponsive PNIPAM and a mineralization controlling block of poly-acrylic acid and the nanocrystal formation kinetics studied by in situ X-ray diffraction.